Appl. Phys. A 65, 251–257 (1997)

Applied Physics A Materials Science & Processing

© Springer-Verlag 1997

Characterization of silicon carbide surfaces of 6H-, 15R- and 3C-polytypes by optical second-harmonic generation in comparison with X-ray diffraction techniques

C. Jordan[1], **H. Schillinger**[1], **L. Dressler**[1], **S. Karmann**[2], **W. Richter**[2], **K. Goetz**[1], **G. Marowsky**[3], **R. Sauerbrey**[1]

[1] Institut für Optik und Quantenelektronik, Friedrich-Schiller-Universität Jena, Max-Wien-Platz 1, 07743 Jena, Germany
(Fax: +49-3641/636-278, E-mail: schillinger@qe.physik.uni-jena.de)
[2] Institut für Festkörperphysik, Friedrich-Schiller-Universität Jena, Max-Wien-Platz 1, 07743 Jena, Germany
(Fax: +49-3641/635-738)
[3] Laser-Laboratorium Göttingen e.V., Hans-Adolf-Krebs-Weg 1, 37077 Göttingen, Germany
(Fax: +49-551/503-599, E-mail: gmarows@gwdg.de)

Received: 16 December 1996/Accepted: 24 March 1997

Abstract. Second-harmonic (SH) generation is a versatile method applicable to in-situ characterization of even non-centrosymmetric media like silicon carbide (SiC). In particular, the azimuthal rotational anisotropy of the SH response from SiC observed in reflection allows identification of various polytypes. The nonlinear-optical results are compared to X-ray diffraction data. The abundance of information obtained through the SH studies makes characteristic fingerprinting of the 6H, 15R, and 3C polytypes of SiC is possible. The spatial resolution of the optical sampling was about 50 μm in the lateral direction with a typical penetration depth of 100 nm for the fundamental radiation. Defect regions of different crystallographic structures in large SiC samples were identified by observing the spatially resolved dependence of the SH intensity.

PACS: 42.65.Nx; 78.66; 42.70.N

Silicon carbide (SiC) is a widely studied semiconductor that crystallizes in over 200 known polytypes. The most common structure is α-SiC, which consists of a mixture of hexagonal polytypes (6H, 4H) and the rhombohedral polytype 15R [1, 2]. Although α-SiC has attracted wide attention because of its potential for applications in the fields of electroluminescence devices and integrated optics [3], very little is known about the nonlinear optical properties of this material.

As already demonstrated in other studies on centrosymmetric materials like silicon, second-harmonic generation (SHG) has proved to be a sensitive tool for studying a large variety of surface and interface structural and electronic properties. Although SHG from non-centrosymmetric materials is not restricted to the surface but is also possible in the bulk material SHG studies in reflection geometry provide substantial crystallographic information on the near-surface region. The generation depth of the second-harmonic (SH) radiation detected in reflection of approximately $\lambda/2\pi$, where λ is the fundamental wavelength, allows higher surface specificity, as compared to the typical interaction lengths of several micrometers in conventional X-ray diffraction techniques in back-reflection geometry (X-ray examination of SiC cf. [4]).

The tensorial properties of the second-order susceptibility, which characterizes the SHG effect, provide information on the crystal structure in case of non-centrosymmetric materials in the near-surface region by investigating its azimuthal rotational anisotropy. Although studies on non-centrosymmetric gallium arsenide (GaAs) demonstrated sensitively surface reconstruction changes [5], hydrogen adsorption [6], and crystal orientation [7] in the rotational anisotropy of the SH response, similar systematic studies were not extended to many other non-centrosymmetric materials. A few investigations on the nonlinear optical properties of SiC were concerned with various components of the second-order nonlinear susceptibility tensor [3, 8–11]. Galeckas et al. [12] investigated bulk samples and epitactic films of 6H-SiC (hexagonal), produced by modified Lely methods and liquid phase epitaxy, and detected crystal imperfections by studying the azimuthal rotational anisotropy of the SH response. Changes in the rotational anisotropy in a particular polarization setting of the incident fundamental and the generated SH beam were demonstrated. However, no comparison with other independent methods was given. Recently, Meyer et al. [13] analyzed epilayers on 6H-SiC and found microcrystallites of 3C-SiC. They demonstrated SH generation as a mapping tool for the detection of inclusions. Also Galeckas et al. [14] showed defects in 3C-SiC films of poor crystallographic quality by using SHG in reflection. In comparison, lifetime measurements of laser-induced carriers by time-resolved reflectivity changes were shown to indicate the quality of the crystalline order.

In the present work, we demonstrate that SHG is a versatile tool to characterize the crystalline structure of SiC. By investigating the rotational anisotropy of the SH response of various polytypes of SiC, we could fingerprint the most important species 6H, 15R and 3C, which are revealed by different crystalline structures. We were also able to distinguish between bulk and surface contributions to the SH signal from cubic and hexagonal SiC by differences in the rotational

anisotropy of the SH intensity, as demonstrated with GaAs samples by Hollering et al. [15]. With regard to the technical application of the SHG-technique as an in-situ probe for crystalline structure, we demonstrate the identification of defect regions in the crystalline structure of large SiC surfaces by using a scanning technique. We verified the results of the SHG studies for each polytype by comparing them with X-ray studies.

1 Experiment

For identification of the crystal structure of the SiC crystals, we studied the reflected SH intensity generated from the SiC surfaces upon irradiation with femtosecond laser pulses. The SH intensity depends sensitively on the relative orientation between the incident electric field and the crystal azimuthal orientation. The use of femtosecond laser pulses allows efficient SHG due to the high peak power and simultaneously there is low thermal loading of the sample [16]. These features and a compact experimental set-up would be attractive for an in-situ characterization method of SiC crystal growth using molecular beam epitaxy (MBE). The details of the experimental set-up are shown in Fig. 1. We used a Kerr-lens mode-locked Ti:sapphire laser oscillator as pump source with 80 fs pulse duration, 83 MHz repetition rate, and a peak power of 110 kW at 800 nm. The pulse train was focused with a spherical mirror onto the SiC sample at an angle of incidence of 45° to generate the frequency doubled radiation in reflection. The laser spot size at the sample surface was set to a fixed diameter of approx. 50 μm. The generated SH radiation at 400 nm was detected with a photomultiplier after blocking the fundamental radiation by color-glass filters (8 mm Schott BG23). The SH signals were registered by a lock-in-amplifier/computer combination. The linearly polarized fundamental laser beam incident on the sample was chopped at 60 Hz to allow noise reduction by lock-in-technique and to decrease the laser-induced heating of the sample. The pump polarization with respect to the SiC sample was set by rotating the sample holder and the filter-detector arrangement around the incoming beam axis, while the polarization of the detected SH signal was analyzed by a Glan polarizer. The SiC samples were rotated around the surface normal using a stepping motor to measure the azimuthal rotational dependence of the SH intensity at various polarization settings of the fundamental and SH radiation.

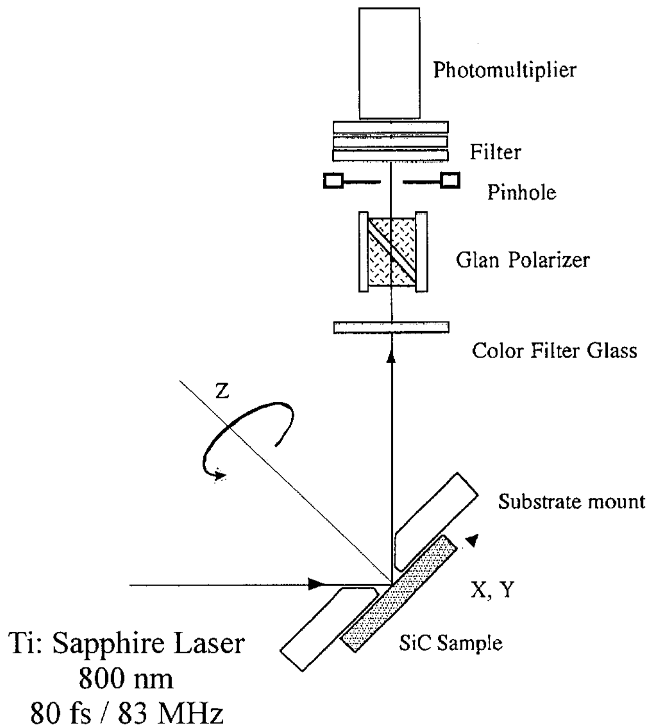

Fig. 1. Experimental set-up for the measurement of azimuthal SH rotation patterns

Special care was taken to avoid detection of the SH radiation from the rearside reflection. The sample holder formed a pinhole of a diameter comparable to the sample thickness (1 mm) to block any rearside reflection. Another pinhole placed close to the photomultiplier discriminated against scattered SH radiation from the crystal volume or the (sometimes unpolished) sample rearside.

In the second part of this study, we investigated the dependence of the SH efficiency on the sample surface position. In this case, the sample was attached to a highly absorbing neutral-density glass plate (Schott NG10) with immersion oil to fill the gap between the glass plate and the sample. This arrangement minimized the rearside-reflected radiation. The sample was scanned by moving it with a computer-controlled x-y-translation stage at a fixed azimuthal angle. To verify the crystallographic findings of the SH experiments, we carried out X-ray diffraction studies of the SiC samples using a conventional Laue apparatus (detection of lattice symmetry). The surface topology was investigated in comparison with the SH scanning technique with an X-ray Lang camera. Both Laue apparatus and Lang camera are described elsewhere [4, 17]. SiC samples of various polytypes and produced by different growth processes were investigated in these experiments. Cubic samples (3C-SiC) were produced in a heteroepitactical growth mode as films of several micrometer thickness on Si(100) substrates using chemical vapor deposition (CVD) [18]. Solid hexagonal samples (6H-SiC) with thickness of approximately 1 mm were grown in Lely- and Acheson-type processes [19]. The epitaxial layers had "as-grown" surfaces, while single crystal samples were polished to optical quality on at least one side. The 6H and 15R sample surfaces were oriented off-axis to a few degrees.

2 Theory

Second-harmonic generation can be described in dipole approximation in terms of a second-order nonlinear polarization

$$P_{\mathrm{i}}(2\omega) = \chi^{(2)}_{ijk} : E_j(\omega) E_k(\omega) \,,$$

where E_{i} describes the incident fundamental electric field amplitude in the irradiated medium and $\chi^{(2)}_{ijk}$ denotes the second-order susceptibility tensor. The symmetry of this tensor is defined by the crystal symmetry of the sample. Therefore different polytypes of SiC are described by different tensors due to their different crystal symmetries. The information on the sample crystal structure can be extracted from the susceptibility tensors by investigating the azimuthal rotational

anisotropy of the SH signals. While SHG in centrosymmetric media is restricted to the sample surface (in the dipole approximation), in non-centrosymmetric media contributions to the SH signal from the bulk material are also allowed. Bulk contributions tend to dominate the generated SH signals because of the longer interaction length of approx. $\lambda/2\pi$ as compared to the surface depth of only a few atomic layers. In general, it is difficult to separate the surface and bulk SH signals since they often show identical rotational symmetry patterns [20].

The normal to all SiC samples defines the z axis, whereas the x and y axes are set in the plane of the sample surface in a manner given by the special symmetry of the polytype. Since we detected the SH radiation in a two-dimensional beam coordinate system which is defined by the radiation-polarization states p and s, a coordinate transformation has to be performed which, in addition, allows for the azimuthal rotation of the sample. The radiation-polarization directions p and s are chosen to be parallel to and perpendicular to the plane of incidence. The SH intensity I is later on defined as I_{mn} in terms of a combination of two polarization states m and n ("m-n rotation pattern"), where m denotes the fundamental and n the polarization of the SH signal. The second-order susceptibility tensors in the crystal coordinate system are listed in many textbooks [2, 21–23]. Since we investigated SiC crystals cut in the (001) plane (cubic) and (0001) plane (hexagonal or rhombohedral), the z axis is coincident with the surface normal and the only transformation operation remaining is a rotation around the z axis. From considerations of the symmetry properties of the different polytypes of the investigated SiC samples, we can easily find the rotational symmetries of the SH response. In Table 1, the crystal classes of several SiC polytypes in the bulk material and in the surface are shown [2]. Also, the azimuthal rotational symmetry of the SLI electric field taken from [5, 24] are listed.

In the following, we briefly discuss the correlation between crystal symmetry and azimuthal rotational anisotropy of the SH response from 3C, 6H, and 15R polytype SiC. Following Neumann's principle, the symmetry of a physical crystal property has to include the symmetry elements of the crystal point group [25]. Therefore, SiC polytypes of different crystal symmetry possess different second-order susceptibility $\chi^{(2)}$ tensors. Since SH signals from SiC originate from both bulk and surface material, the symmetry properties of both contributions have to be studied. The effective SH generation lengths in the surface and in the bulk material suggest a dominance of the bulk signal. Different symmetries in cubic 3C-SiC(001) bulk and surface material allow to distinguish between the bulk and surface SH contributions due to the different rotational anisotropy. Furthermore, crystal surface defects cause additional symmetries in the azimuthal anisotropy of the surface SH signals, that also allow the distinction between surface and bulk contributions. The following SH azimuthal rotational symmetries are expected from the 3C, 6H- and 15R polytypes of SiC:

(a) 3C-SiC(001) has different crystal symmetries in the bulk material ($\overline{4}3m$) compared to the sample surface ($4mm$) [11]. In the bulk material, a 4-fold rotation-reflection axis parallel to the surface normal is apparent [26], which corresponds to a 2-fold rotational axis. Since a 2-fold rotational symmetry appears in various components of the nonlinear susceptibility tensor, the 2-fold symmetry shows up also in the SH electric field. These components convert to a 4-fold symmetry in the SH intensity, measurable in particular polarization settings (Table 1). The surface possesses a full 4-fold rotational crystal symmetry, which cannot be displayed in the SH rotational anisotropy in the dipole approximation [27]. Accordingly, the contributions from the surface to the SH electric field and intensity are purely isotropic.

(b) 6H-SiC(0001) crystals show identical crystal rotational symmetries (6 mm) in the surface and bulk material. The hexagonal crystal structure possesses a 6-fold rotational symmetry around the surface normal, which cannot be resolved in the azimuthal anisotropy of the SH response in the dipole approximation. Therefore, no azimuth angle dependent SH signal is expected from the ideal hexagonal crystal. Defects in the surface (defects in the bulk crystal structure are less probable), however, may cause anisotropic contributions to the SH signal.

(c) 15R-SiC(0001) has a rhombohedral crystal symmetry in the bulk as well as in the surface atomic structure. Around the surface normal, the crystal structure as well as the second-order nonlinear susceptibility have a 3-fold rotational invariance. Since isotropic components are apparent also in the susceptibility tensor, the SH electric field consists of a coherent superposition of anisotropic 3-fold and isotropic contributions in selected polarization settings (Table 1). By squaring the electric field amplitude to evaluate the SH intensity, a superposition of 3-and 6-fold azimuthal rotational symmetry contributions appears.

3 Results and discussion

3.1 Azimuthal anisotropy

In the following, we demonstrate that a polytype specific fingerprint for three polytypes 3C, 6H, and 15R of SiC can be derived from a study of the rotational anisotropy of the SHG

Table 1. Azimuthal and electric field symmetry for bulk and surface of 3C, 6H, and 15R SiC crystals. The angle α denotes the azimuthal rotation angle, while the arbitrary phase Φ relates the azimuthal crystal orientation to the experimental starting angle at 0°

	SiC(001) 3C		SiC(000) 6H	SiC(0001) 15R
	surface	bulk	surface/bulk	surface/bulk
Crystal class	cubic $4mm$	cubic $\overline{4}3rm$	hexagonal $6mm$	rhomboedric 3
azimuthal symmetry	4-fold	2-fold	6-fold	3-fold
E-field symmetry:				
p-p	const.	$\cos(2\alpha+\Phi)$	const.	$\text{const.}+\cos(3\alpha+\Phi)$
p-s	–	$\cos(2\alpha+\Phi)$	–	$\cos(3\alpha+\Phi)$
s-p	const.	$\cos(2\alpha+\Phi)$	const.	$\text{const.}+\cos(3\alpha+\Phi)$
s-s	–	–	–	$\cos(3\alpha+\Phi)$

in four polarization settings. In Fig. 2a–d, the SH intensity from a 3C-SiC(001) film is shown as a function of the azimuthal orientation for the four different polarization settings. In all polarization combinations, a dominant 4-fold rotational symmetry is shown without any visible 2-fold symmetry which would originate from an additional isotropic contribution. In the pp, ps, and sp polarization combinations, the displayed 4-fold symmetry fits well with the theoretical expectations, while in the ss polarization no SH signal is to be expected from theory contrary to the experimentally obtained result. The relative SH amplitudes for the different polarization settings, additionally shown in Fig. 2, indicate the low conversion efficiency for the ss-polarization. This contribution is presumably a quadrupolar signal from the bulk material.

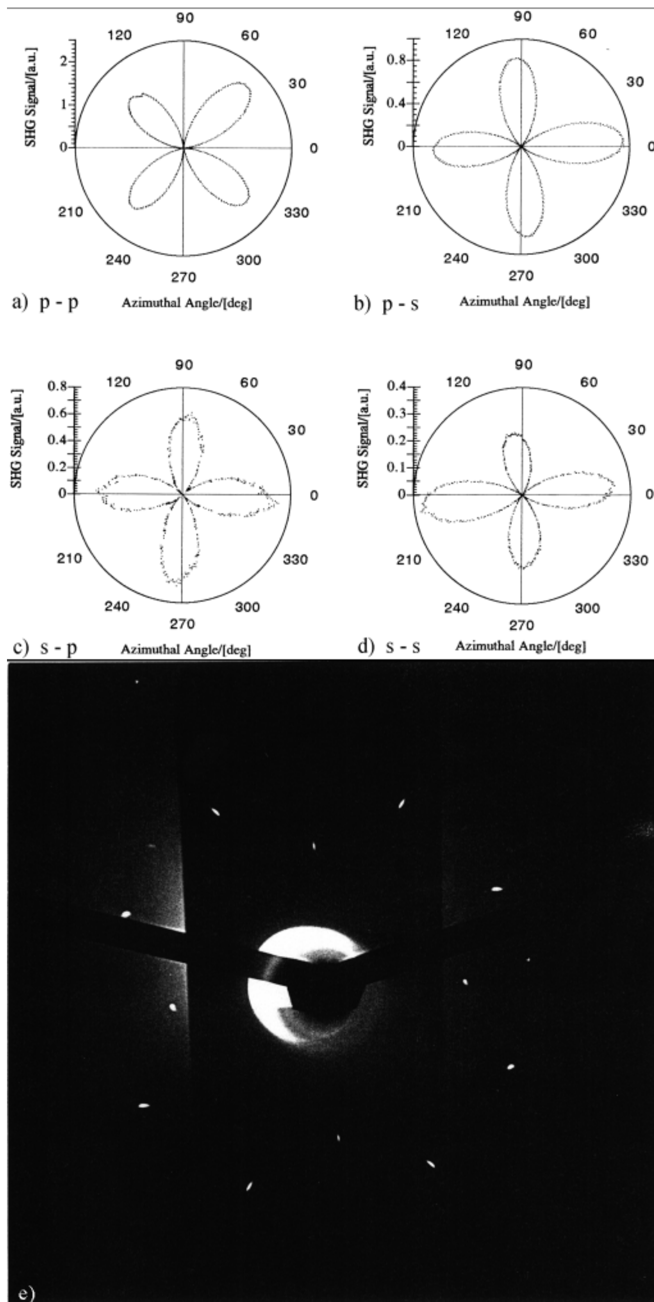

Fig. 2a–e. SH signal dependence of 3C-SiC(001), grown on a Si(001) substrate by CVD method, on the azimuthal rotation angle. Polarization combinations (fundamental-SH) were **a** p-p **b** p-s **c** s-p **d** s-s. **e** X-ray diffraction (Laue) picture from the same sample as studied by SH measurements. The Si(001) substrate was removed by etching for this measurement

Additional investigations on Si(100) confirmed that no SH signal from the substrat – as predicted by symmetry considerations – could be detected.

Figure 2e shows the corresponding Laue picture of the 3C-SiC(001) film in transmission geometry. By studying the central peaks of the Laue picture, a 4-fold rotational symmetry is apparent which is in good agreement with the SH investigation.

Figure 3a–d shows the azimuthal rotational pattern of the SH intensity from hexagonal 6H-SiC(0001) Lely-type samples in four polarization combinations. It is possible to classify two types of SH rotation patterns. In the pp and sp polarizations the SH signals show dominant isotropic contributions, as expected from theory. However, in the ps and ss polarizations dominant 2-fold symmetries are obtained, although no signals are expected from theory. The signal amplitudes in the ps and ss polarizations are considerably smaller than for those polarizations where the theory predicts a signal. In studies of the crystallographic structure of silicon surfaces, the occurrence of unexpected 2-fold symmetry components in the SH rotational pattern is known to originate from steps and terraces in the surface plane [28]. In the same manner, we may describe the 2-fold symmetry components in the SH anisotropy to be due to steps. In the pp and sp polarizations, these effects are not noticeable due to the strong isotropic SH contributions from the bulk material.

Figure 3e shows the corresponding Laue-picture of the same 6H-SiC(0001) sample. A clear 6-fold rotational symmetry is shown by the inner ring of X-ray reflections, which fits well with the results of the SH rotational symmetry analysis in the pp and ps polarization combinations. Due to the transmission geometry, it is not possible to resolve surface defects by the Laue-technique. Even in the grazing incidence geometry, as used in other arrangements, the interaction length is much more than 1 μm.

In Fig. 4a–d, the SH rotation pattern from a large rhombohedral 15R-SiC(0001) Lely platelet are shown for the pp, ps, sp and ss polarization combinations. Similar to the hexagonal 6H-SiC, two classes of SH rotation patterns are apparent. The dominant 3-fold symmetry in the pp and sp SH intensity rotation patterns is possibly due to a coherent superposition of the isotropic and 3-fold rotational contributions in the SH electric field. In the ps and ss polarization combinations, dominant 6-fold rotational symmetries of the SH signals are apparent, which fits well with the theoretical expectations according to Table 1. Deviations from the 6-fold symmetry can be explained by surface defects, like steps, which induce additional (2-fold) symmetry contributions. The relatively small SH signal amplitude from the surface defects shows the dominance of the bulk signal over the surface signal.

For comparison, the corresponding Laue picture of the 15R-SiC(0001) sample in transmission geometry is shown in Fig. 4e. In the central region of the diffraction pattern, a 3-fold rotational symmetry is apparent which fits well with the theoretical expectations and the results of the SH studies. In addition, we can deduce from the good quality of the diffrac-

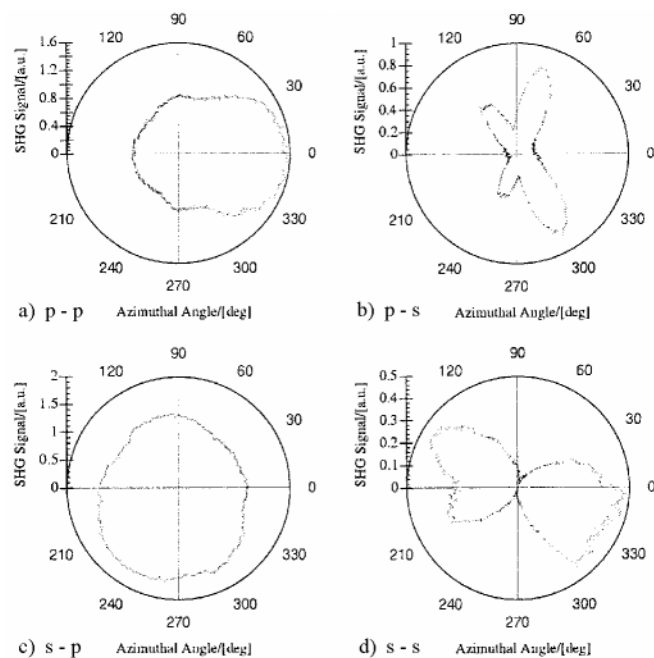

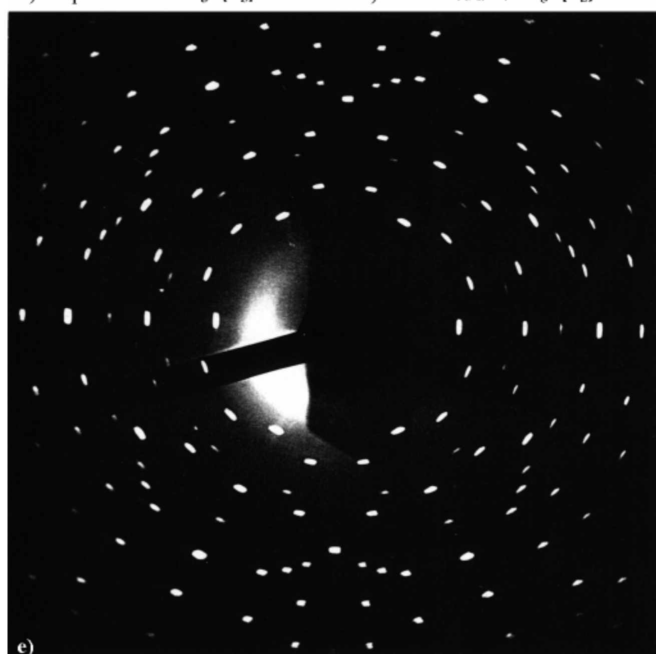

Fig. 3a–e. SH signal dependence of 6H-SiC(0001), grown by the modified Lely method, on the azimuthal rotation angle. Polarization combinations (fundamental-SH) were **a** p-p **b** p-s **c** s-p **d** s-s. **e** X-ray diffraction (Laue) picture from the same sample

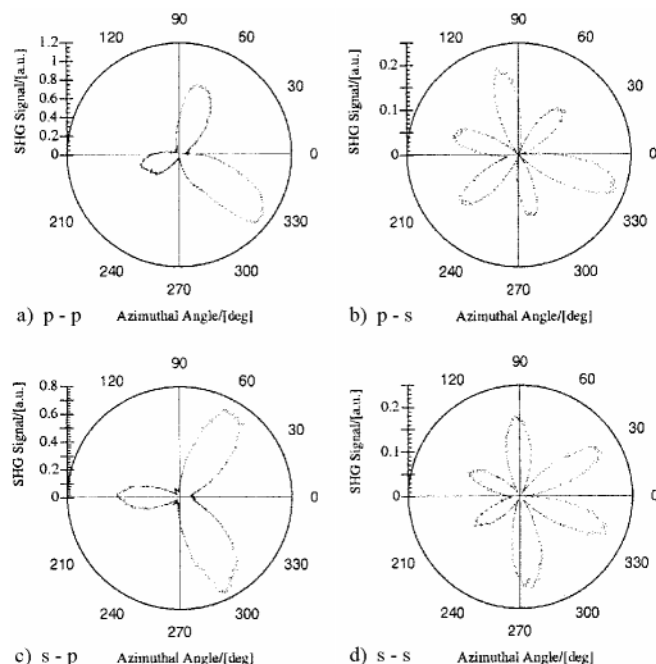

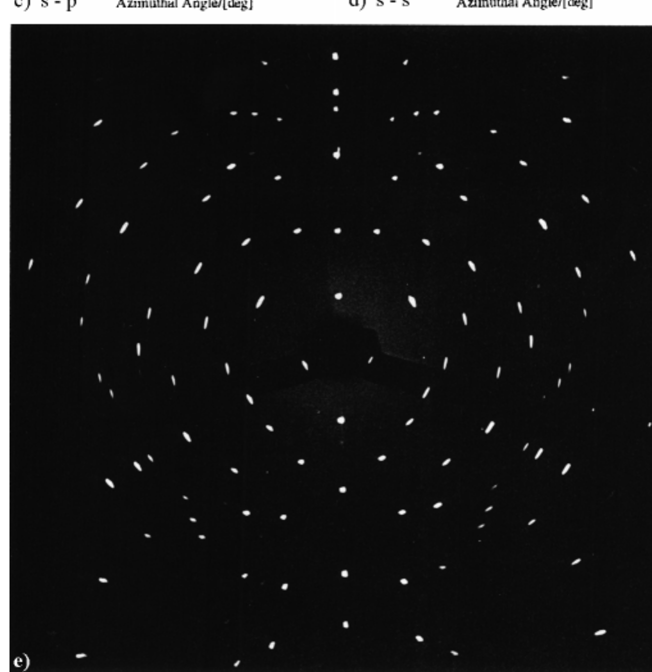

Fig. 4a–e. SH signal dependence of 15R-SiC(0001), grown by modified Lely method, on the azimuthal rotation angle. Polarization combinations (fundamental-SH) were **a** p-p **b** p-s **c** s-p **d** s-s. **e** X-ray diffraction (Laue) picture from the same sample

tion pattern of the Laue pictures that all of the investigated SiC samples had good monocrystalline quality.

In conclusion, we demonstrated characteristic fingerprint-type nonlinear-optical properties for the different SiC-polytypes in the SH azimuthal rotational anisotropy, which were also confirmed by X-ray Laue pictures. By using a focused laser beam, we achieved a spatial resolution of approximately 50 μm on the sample surface and a minimal resolution of a Fresnel depth of roughly $\lambda/2\pi$. The study of crystalline cubic and hexagonal SiC samples at certain polarization combinations allowed the separation of bulk and surface SH contributions [28].

3.2 Surface topography

Technical applications of SiC require full surface characterization of the samples with a high spatial resolution. The results of SHG scanning experiments demonstrate this capability. We investigated the spatial dependence of the SH intensity from azimuthally fixed hexagonal 6H-SiC(0001) Boule-type samples. In addition, we used an X-ray diffraction technique (Lang camera) for comparison with the results of the SH studies. In Fig. 5a, the spatial dependence of the SH intensity in pp polarization from a limited area a 6H-SiC(0001) sample

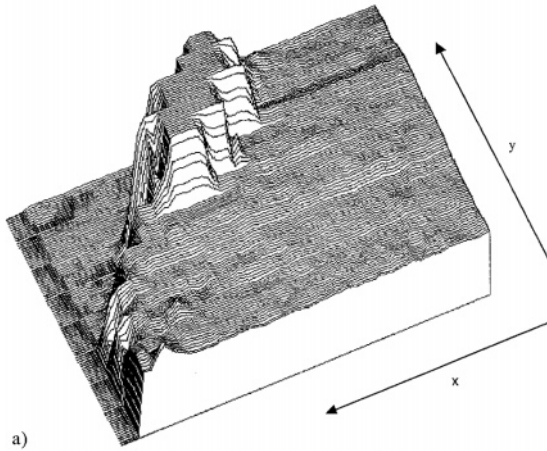

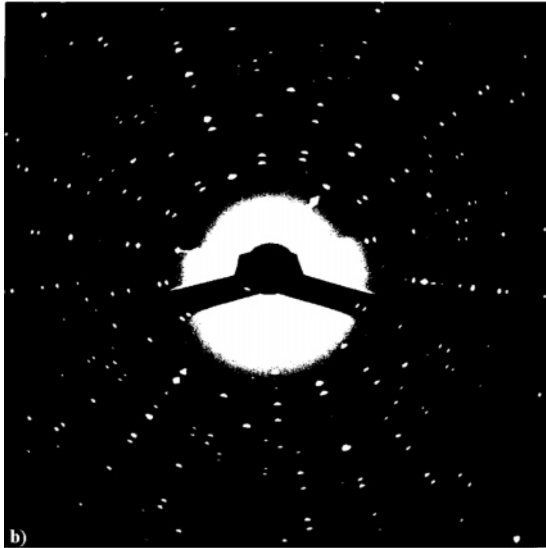

Fig. 5. a Contour plot of a SHG scan across a 6H-SiC(0001) Lely-type sample. The height of the contour is proportional to the p-p signal at a fixed azimuthal angle. The step-like structure in the y direction is due to the limited step-width in this dimension. **b** X-ray diffraction (Laue) picture from the defect region of this sample. The defect was identified as change to the 15R polytype. **c** X-ray topograph of the same sample recorded with a Lang camera. The same defect region appears as a spot with virtually no X-ray signal due to the change in the character of the polytype

is shown as a contour plot where the x and y axes define the coordinates on the sample surface and the z axis indicates the SH intensity. The surface scan shows an area of nearly constant and low SH efficiency, which extended over the whole surface except for a limited joined "defect" region characterized by a several times higher efficiency. By an additional Laue-investigation (Fig. 5b), we could identify the defect region to consist of a different crystal structure. While the whole sample showed an ideal hexagonal 6H-SiC polytype, in the defect region the polytype changes to an ideal rhombohedral 15R-structure. In Fig. 5c, an X-ray topograph of the corresponding SiC surface is shown, which was generated in reflection with a Lang camera. In this topograph, the same defect region is identified by a total lack of the X-ray signal apart from some other less prominent defects. The otherwise homogeneous picture corroborates that besides the defect, the crystal is highly ordered and of good quality.

We could therefore identify the change in the polytype from 6H to 15R by an increase in the SH efficiency. We could verify such changes of polytype in various samples whereas no change in the optical properties was visible. A different indication of a defect region in a spatial scan of a 6H-SiC(0001) sample is shown in Fig. 6. The dependence of the SH intensity on the sample surface position is plotted as a contour plot. A nearly constant SH efficiency can be seen over the whole surface except for a line-shaped region where it decreases strongly. A Laue picture of the defect region identified the crystal structure to be a superposition of 6H and 15R polytype structures.

4 Conclusion

We have shown for the first time the fingerprints of different polytypes of SiC in the azimuthal rotational anisotropy of second-harmonic radiation generated in the near-surface region. Although SiC is non-centrosymmetric, we demon-

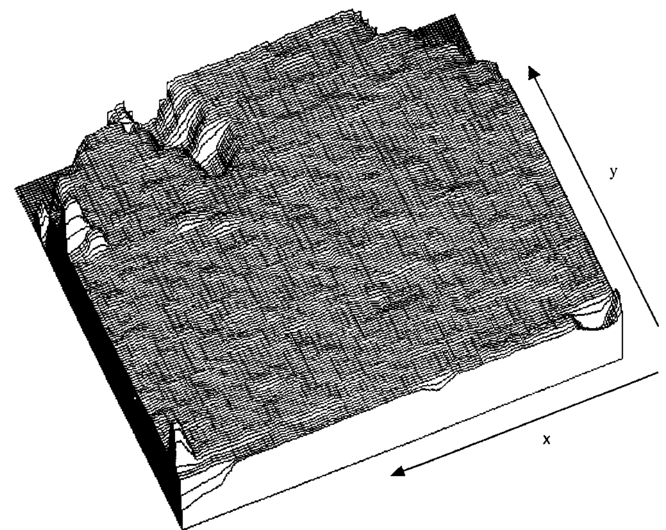

Fig. 6. Contour plot of a SHG scan across a 6H-SiC(0001) Lely-type sample. The height of the contour is again proportional to the p-p signal at a fixed azimuthal angle. The valley-like defect region (*lower signal*) in the *upper-middle* part was later identified as a 15 R rotational twin by X-ray diffraction (Laue method)

strated for some polytypes a discrimination of the bulk SH signals and a possible detection of surface contributions due to different crystalline symmetries. In these cases, even crystallographic defects in the surface, such as steps and kinks, were observed. In comparison with X-ray Laue pictures in transmission, we could verify all crystallographic information obtained from studying the SH rotation patterns. Due to the different efficiencies in the SH generation from different polytypes of SiC, we were able to detect areas of different polytypes in large samples by a spatial scanning technique. The different SH efficiencies of the different polytypes allowed us to identify the specific polytype. We verified the existence of defect areas by X-ray diffraction using a Lang camera and identified the corresponding crystal defect structure with a Laue apparatus.

Acknowledgements. The authors would like to thank Nils Nordell from IMC, Kista, and Lea DiCioccio from LETI, Grenoble, for providing us with the SiC samples. This work was supported by the Deutsche Forschungsgemeinschaft in the framework of SFB 196, Teilbereiche A3, B9, and C1. The authors thank J. Jethwa and P. Tregel, Göttingen, for a critical reading of the English version of this manuscript.

References

1. F. Schröder (ed.): *Gmelin Handbook of Inorganic Chemistry, Silicon*, Part B3, (Springer-Verlag, Berlin, Heidelberg, New York 1987)
2. K.-H. Hellwege, O. Madelung (eds.): *Landolt Börnstein New Series* III/17c, (Springer-Verlag, Berlin, Heidelberg, New York, Tokyo 1982) pp403
3. P.M. Lundquist, W.P. Lin, G.K. Wong, M. Razeghi, J.B. Ketterson: Appl. Phys. Lett. **66**, 1883 (1995)
4. L. Dressler, K. Goetz, J. Kräußlich: Phys. Status Solidi (a) **148**, 81 (1995)
5. Ch. Yamada, T. Kimura: Phys. Rev. Lett. **70**, 2344 (1993)
6. S.R. Armstrong, M.E. Pemble, A. Stafford, A.G. Taylor: J. Phys: Codens. Matter **3**, 363 (1991)
7. D.J. Bottomley, O. Lüpke, J.O. Mihaychuk, H.M. van Driel: J. Appl. Phys. **74** (10), 6072 (1993)
8. S. Singh, J.R. Potopowicz, L.O. van Uitern, S.H. Wemple: Appl. Phys. Lett. **19**, 53 (1971)
9. J. Chen, Z.H. Levine, J.W. Wilkins: Phys. Rev. B **50**, 11514 (1994)
10. R.A. Soref: J. Appl. Phys. **72**, 626 (1992)
11. G.L. Harris, E.W. Jones, M.G. Spencer, K.H. Jackson: Appl. Phys. Lett. **59**, 1817 (1991)
12. A. Galeckas, M. Petrauskas, H. Bergner, R. Görlich, A. Krause, M. Willander: Phys. Status Solidi (a) **151**, 219 (1995)
13. C. Meyer, O. Lüpke, E. Stein von Kamienski, A. Golz, H. Kurz: Appl. Phys. Lett. **69**, 2243 (1996)
14. A. Galeckas, M. Petrauskas, Q. Wahab, M. Willander: Nucl. Instrum. Methods Phys. Res. B **65**, 357 (1992)
15. R.W.J. Hollering, M. Barmentlo: Opt. Commun. **88**, 141 (1992)
16. J.I. Dadap, X.F. Hu, N.M. Russell, J.O. Ekerdt, J.K. Lowell, M.C. Downer: IEEE J. STQE *1*, 1145 (1995)
17. B.K. Vainshtein: Modern Crystallography, Vol.1, *Fundamentals of Crystals*, (Springer-Verlag, Berlin, Heidelberg, New York 1994)
18. N. Becourt, PhD Thesis, University of Montpellier, France (1993)
19. S. Karmann, PhD Thesis, University of Erlangen, Germany (1992)
20. P. Guyot-Sionnest, Y.R. Shen: Phys. Rev. B **42**, 9263 (1988)
21. F. Zernike, J.E. Midwinter: *Applied Nonlinear Optics*, (Wiley Interscience, New York 1973) pp.61–67
22. P.N. Butcher, D. Cotter: *The elements of nonlinear optics* (Cambridge University Press 1990) pp.299–305
23. Y.R. Shen: *The principles of nonlinear optics* (Wiley-Intersience, New York 1984)
24. J.E. Sipe, D.J. Moss, H.M. van Driel: Phys. Rev. B **35**, 1129 (1987)
25. J.F. Nye: *Physical Properties of Crystals* (Clarendon Press, Oxford 1959)
26. N.W. Ashcroft, N.D. Mermin: *Solid State Physics*, (Saunders College, Philadelphia 1976), p.119
27. B. Koopmans, F. van der Woude, G.A. Sawatzky: Phys. Rev. B **46**, 12780 (1992)
28. C.W. van Hasselt, M.A. Verheijen, Th. Rasing: Phys. Rev. B **42**, 9263 (1990)